Progress In Electromagnetics Research C, Vol. 63, 163–171, 2016

Influence of Environmental Conditions on EMF Levels in a Span of Overhead Transmission Lines

Oleksandr Okun[1, *], Yurii Kravchenko[1], and Leena Korpinen[2]

Abstract—The paper is devoted to the investigation of electromagnetic field distribution in the vicinity of overhead transmission lines under different environmental conditions, taking into account the wire sag curve in a span. A wire state equation is utilized, which allows one to calculate stresses in the wire and sags based on the known stresses and temperatures in the initial state. The results of the electric and magnetic field distribution on sample 330 kV and 110 kV transmission lines are presented. We show that the highest electromagnetic field levels are associated with the most severe environmental conditions, resulting in the highest sag.

1. INTRODUCTION

Usually, electric and magnetic field (EMF) measurements generated by high voltage overhead transmission lines (OTLs) are conducted in a warm season (spring–summer). This is due to the limited operating temperature ranges of meters/field analyzers, which do not cover ambient air temperatures below zero. Therefore, execution of field measurements in a warm season does not always guarantee obtaining the highest EMF levels. Especially, it has an impact on long span length, for which the wire length and the sag are significantly varied and the difference can exceed several meters.

The task of calculation and measurement of the EMF levels produced by OTLs has been widely covered in a variety of sources. In spite of this, no due attention on environmental conditions and mechanical calculations within the framework of EMFs has been given. Mainly, this attention has been reduced to the use of the fixed height or application of the wire sag curve in different forms. For instance, in papers [1–4], an OTL was represented as straight horizontal conductors, allocated at the given constant height. The authors of a paper [5] proposed an exact solution and an approximate equation of the catenary for MF calculations. It was shown that the approximation, which assumes a wire as a straight and horizontal conductor with the height varied at each point and equaled to the height of the catenary or the parabola, provides satisfactory accuracy (5%). In order to calculate EMF distributions, complete integration techniques and approaches with catenary approximation were proposed in [6–10]. In [11], the effect of temperature on EMF levels was calculated using alteration of wire length in the span and the linear expansion temperature coefficient, which does not enable us to take into account ice and wind loads.

Based on these studies, the aim of the work is to investigate the influence of environmental conditions on EMF values, generated by high voltage OTLs, with the use of equations considering temperature, ice deposits and wind loads.

Received 11 February 2016, Accepted 20 April 2016, Scheduled 3 May 2016

* Corresponding author: Oleksandr Okun (alexandr.okun@gmail.com).

[1] LLC Soyuzenergoproekt, Kharkiv, Ukraine. [2] Department of Electronics and Communications Engineering, Tampere University of Technology, Tampere, Finland.

2. MATERIALS AND METHODS

2.1. Mechanical Calculations

If we approximately assume that the weight of a wire is uniformly distributed in the horizontal direction and not along the length of the wire as it actually occurs, the sag wire curve is a parabola with the vertex at the origin of coordinates. If, however, we accept that the wire weight is uniformly distributed along its length, then we obtain a catenary equation for the sag curve.

Table 1 summarizes basic expressions and equations that describe the parameters of a wire represented in the form of the parabola and the catenary for the case of equal suspension height.

Table 1. Basic equations for a wire represented in the form of the parabola and the catenary.

Parabola	Catenary
Wire sag curve equation	
$y(x) = \frac{\gamma \cdot x^2}{2 \cdot \sigma}$ (1)	$y(x) = \frac{\sigma}{\gamma}\left(\cosh \frac{x \cdot \gamma}{\sigma} - 1\right)$ (4)
The sag of a wire	
$f = \frac{\gamma \cdot l^2}{8 \cdot \sigma}$ (2)	$f = \frac{\sigma}{\gamma}\left(\cosh\left(\frac{l \cdot \gamma}{2 \cdot \sigma}\right) - 1\right)$ (5)
The length of a wire in a span	
$L = l + \frac{\gamma^2 \cdot l^3}{24 \cdot \sigma^2}$ (3)	$L = 2\left(\frac{\sigma}{\gamma}\sinh\left(\frac{l \cdot \gamma}{2 \cdot \sigma}\right)\right)$ (6)

where σ is the stress, MPa; γ is the specific load, MPa/m; ℓ is the span length, m.

It should be noted that the catenary, for the purpose of computation, is less convenient than the parabola. Moreover, the accuracy of the equation for the catenary and parabola is almost the same [5]. Therefore, while the mechanical wire calculations in practice are performed with the parabola; the catenary is recommended to use for very long spans (700–1000 m).

In order to determine values of stresses and wire sags under different operation conditions, a dependence of the stress from the load is expressed in the form of an equation, which is called the wire state equation. Equation (7) represents the wire state equation, received for the parabola; Equation (8) is for the catenary.

$$\sigma - \frac{\gamma^2 \cdot E \cdot \ell^2}{24 \cdot \sigma^2} = \sigma_o - \frac{\gamma_o^2 \cdot E \cdot \ell^2}{24 \cdot \sigma_o^2} - \alpha \cdot E \cdot (t - t_o), \tag{7}$$

$$\sigma - \frac{2E \cdot \sigma}{l \cdot \gamma}\sinh\left(\frac{l \cdot \gamma}{2 \cdot \sigma}\right) = \sigma_o - \frac{2E \cdot \sigma_0}{l \cdot \gamma_0}\sinh\left(\frac{l \cdot \gamma_0}{2 \cdot \sigma_0}\right) - \alpha \cdot E \cdot (t - t_o), \tag{8}$$

where σ, γ, t are the stress, MPa, the specific load, MPa/m and the temperature, °C, consequently, in the final observation state; σ_o, γ_o, t_o are the stress, the specific load and the temperature, consequently, in the initial state; ℓ is the span length, m; α is the linear expansion temperature, K^{-1}; E is the elastic modulus, MPa.

Using Equations (7) and (8), stresses in the wire can be found at any required condition based on the known stresses and temperatures in the initial state.

For mechanical calculations, any state can be taken as an initial state characterized by a temperature and a load. However, it is necessary to maintain the stress within the allowable limits under the minimum temperature and the highest load, as well as under the annual average temperature. In order to comply with the given basic condition, it is most correct to accept as the initial state one of the modes in which the stress in the wire can be set equal to the permissible stress [12].

Values of the linear expansion temperature coefficient α and the elastic modulus E are derived from design parameters data as well as by means of a calculation from formulae (9) and (10) for aluminum conductor steel reinforced (ACSR) wires.

$$E = E_c \frac{1 + km}{1 + k}, \tag{9}$$

where $k = \frac{F_a}{F_c}$; $m = \frac{E_a}{E_c}$; F_a is the section of aluminum; F_c is the section of steel; E_a is the elastic modulus of aluminum ($6.3 \cdot 10^4$ MPa); E_c is the elastic modulus of steel ($20 \cdot 10^4$ MPa);

$$\alpha = \alpha_c \frac{1 + kmn}{1 + k}; \tag{10}$$

where $n = \frac{\alpha_a}{\alpha_c}$; α_a is the linear expansion temperature coefficient of aluminum ($23 \cdot 10^{-6}\,\mathrm{K}^{-1}$); α_c is the linear expansion temperature coefficient of steel ($12 \cdot 10^{-6}\,\mathrm{K}^{-1}$).

For convenience of employing the wire sag curve for EMF calculations, it is possible to write Equation (1) as assigned to the axes indicated in Figure 1, taking into account (2) in the form (11).

$$y(x) = H_0 + \frac{\gamma \cdot \left(x - \frac{l}{2}\right)^2}{2 \cdot \sigma} = H_0 + f + \frac{4fx^2}{l^2} - \frac{4fx}{l} = H_S - \frac{4fx}{l}\left(1 - \frac{x}{l}\right), \tag{11}$$

where H_0 is the height in the mid-span, m; H_S is the suspension height, m.

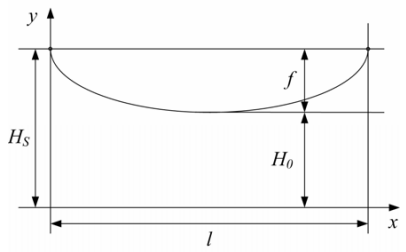

Figure 1. The wire sag curve (f is the sag; H_0 is the height in the mid-span; H_S is the suspension height; $\ell$is the span length).

In the same way, Equation (4) can be rewritten as follows:

$$y(x) = H_0 + \frac{\sigma}{\gamma}\left(\cosh\frac{\left(x - \frac{l}{2}\right) \cdot \gamma}{\sigma} - 1\right). \tag{12}$$

2.2. EMF Calculations

Generally, the task of EMF calculation in a span of an overhead transmission line requires three-dimensional modeling with the use of numerical methods. Nevertheless, it is possible to obtain satisfactory accuracy of calculated results by means of two-dimensional approaches with the height variation along the span, demonstrated in [5, 7].

Based on these approaches, in order to obtain the distribution of EMFs in the span, it is necessary to use Equations (11) or (12) for computing the height of wire H at every calculation point. The resulting value of the EF intensity E and magnetic flux density B at the desired point can be found by summing the x, y vector components of the intensities Ex, Ey, and Bx, By, respectively

$$E = \sqrt{\mathrm{Re}\left(\sum \dot{E}x_i\right)^2 + \mathrm{Im}\left(\sum \dot{E}x_i\right)^2 + \mathrm{Re}\left(\sum \dot{E}y_i\right)^2 + \mathrm{Im}\left(\sum \dot{E}y_i\right)^2}, \tag{13}$$

$$B = \sqrt{\mathrm{Re}\left(\sum \dot{B}x_i\right)^2 + \mathrm{Im}\left(\sum \dot{B}x_i\right)^2 + \mathrm{Re}\left(\sum \dot{B}y_i\right)^2 + \mathrm{Im}\left(\sum \dot{B}y_i\right)^2}, \tag{14}$$

where

$$\dot{E}x_i = \frac{\dot{q}_i}{2\pi\varepsilon\varepsilon_0}\left(\frac{x \pm xd_i}{(x \pm xd_i)^2 + (H_i - h)^2} - \frac{x \pm xd_i}{(x \pm xd_i)^2 + (H_i + h)^2}\right), \tag{15}$$

$$\dot{E}y_i = \frac{\dot{q}_i}{2\pi\varepsilon\varepsilon_0}\left(\frac{H_i - h}{(x \pm xd_i)^2 + (H_i - h)^2} + \frac{H_i + h}{(x \pm xd_i)^2 + (H_i + h)^2}\right), \tag{16}$$

$$\dot{B}x_i = \frac{\mu\mu_0 I_i}{2\pi}\left(\frac{H_i - h}{(x \pm xd_i)^2 + (H_i - h)^2}\right) \tag{17}$$

$$\dot{B}y_i = \frac{\mu\mu_0 I_i}{2\pi}\left(\frac{x - d_i}{(x \pm xd_i)^2 + (H_i - h)^2}\right). \tag{18}$$

q_i are the charges on the conductors, C/m; x is the distance from the y-axis to the observation point, m; xd_i is the distance between the y-axis and the axis of the i-th conductor, m; H_i is the height of the i-th conductor, obtained with (11) or (12), m; h is the height of the observation point (plane) above the ground surface, m; ε_0 is the permittivity of vacuum ($8.854 \cdot 10^{-12}$ F/m); $\varepsilon = 1$ is the permittivity of air; I_i is current in the i-th conductor; μ_0 is the permeability of vacuum ($4\pi \cdot 10^{-7}$ H/m); $\mu = 1$ is the permeability of air.

The charges q_i on the conductors are determined through the voltages U_j and the Maxwell potential coefficients with the system of potential equations

$$\dot{U}_j = \sum_{i=1}^{k} p_{ji}\dot{q}_i, \quad j = 1, 2 \ldots k, \tag{19}$$

where p_{ii} are the self ($i = j$) and mutual ($i \neq j$) potential coefficients

$$p_{ii} = \frac{1}{2\pi\varepsilon}\ln\left(\frac{2He_i}{r_i}\right), \quad p_{ij} = \frac{1}{2\pi\varepsilon}\ln\left(\frac{D'_{ij}}{D_{ij}}\right); \tag{20}$$

He_i is the average suspension height of the i-th conductor, m; r_i is radius of the i-th conductor, m; D_{ij} is the distance between the i-th and$j$-th conductor, m; D'_{ij} is the distance between the i-th conductor and the j-th image conductor, m.

2.3. Parameters of 330 kV and 110 kV OTLs under Study

In order to investigate the influence of environmental conditions, two OTLs were chosen that have different phase conductor arrangements and different rated voltages. The first object is a 330 kV line with 2xACSR 400/51 conductors, while the second one is a 110 kV line with ACSR 120/19 conductors. Mechanical and other characteristics of these OTLs as well as environmental conditions for the Kharkiv region in Ukraine are presented in Tables 2–4. These parameters and characteristics are possible to get from regulations, district classification, and manufacturer data. Specific loads can be obtained directly or by means of calculations, using well-known formulae from, for example, [12].

Table 2. Environmental conditions according to district classification of the Ukraine territory.

Temperature, °C	Average annual	+7
	Maximum	+38
	Minimum	−40
	In time of ice deposits	−5

3. RESULTS OF CALCULATIONS

Based on parameters presented in Tables 2–4 and equations from the second chapter, the EMF levels under 330 kV and 110 kV OTLs for all design modes with specific loads and corresponding temperatures were calculated. Table 5 presents the results of sag calculation for different design modes. An example of EF and MF distribution for the 330 kV line at a temperature of 20°C is presented in Figure 2. Figure 3 shows the calculated relationship between sag, stress, and temperature. The results of EMF calculations at the maximum, the minimum, and the average annual temperatures as well as ice deposits are presented in Figures 4–7. In the calculations of the MF, it is assumed that the current is equal to 500 A for 330 kV OTL and 150 A for 110 kV OTL. The height of the observation point above the ground surface is 1.8 m.

Table 3. Parameters of 330 kV and 110 kV OTLs.

Parameters	330 kV OTL	110 kV OTL
Arrangement of the phase conductors	horizontal	triangular
Number of the sub-conductors n	2	1
Distance between the phase conductors d, m	8	d12 = 5.5; d23 = 4.27; d13 = 6.8
Bundle spacing a, cm	40	–
Length of the span l, m	400	240
Permissible clearance value in unpopulated areas, m	7.5	6
Suspension height H_s, m	19.5	$H_{s1} = H_{s2} = 13.1$; $H_{s3} = 17.1$
Sag of the wires at a temperature of 20°C, f, m	10	6.3

Table 4. Mechanical parameters of wires and loads.

Parameters, unit	Values	
	ACSR 400/51 type	ACSR 120/19 type
Elastic modulus E, MPa	$7.7 \cdot 10^4$	$8.25 \cdot 10^4$
Linear expansion temperature coefficient α, K^{-1}	$19.8 \cdot 10^{-6}$	$19.2 \cdot 10^{-6}$
Mass, kg/km	1490	471
Specific load due to the wire dead weight γ_1, MPa/m	$3.28 \cdot 10^{-2}$	$3.38 \cdot 10^{-2}$
Specific load due to the weight of ice deposits on the wire γ_2, MPa/m	$3.51 \cdot 10^{-2}$	$8.46 \cdot 10^{-2}$
Specific load due to the wire dead weight with ice deposits γ_3, MPa/m	$6.79 \cdot 10^{-2}$	$11.84 \cdot 10^{-2}$
Specific load under the action of the wind to the wire without ice deposits γ_4, MPa/m	$3.47 \cdot 10^{-2}$	$6.42 \cdot 10^{-2}$
Specific load under the action of the wind to the wire, covered with ice deposits γ_5, MPa/m	$1.99 \cdot 10^{-2}$	$3.49 \cdot 10^{-2}$
Specific load due to the wire dead weight and under the action of the wind to the wire without ice deposits γ_6, MPa/m	$4.78 \cdot 10^{-2}$	$7.25 \cdot 10^{-2}$
Specific load under the action of the wind to the wire, covered with ice deposits, the dead weight and the weight of ice deposits γ_7, MPa/m	$6.7 \cdot 10^{-2}$	$11.53 \cdot 10^{-2}$
Ultimate tensile stress σ_p, MPa	280	290
Permissible stress when exposed to the maximum load or under the minimum temperature σ_{H6}, MPa	126	120
Permissible stress under the average annual temperature σ_{cp}, MPa	84	90
Radius of the wirer_0, m	0.01375	0.0076

Table 5. Calculated sags for different design modes.

Type of OTL	Calculated sag values in meters for design modes with:					
	γ_1 and max t	γ_1 and min t	γ_1 and average t	γ_3 and $-5°C$	γ_6 and $-5°C$	γ_7 and $-5°C$
330 kV line	10.80	7.02	9.33	10.78	9.72	10.75
110 kV line	6.80	4.37	5.90	7.1	6.36	7.06

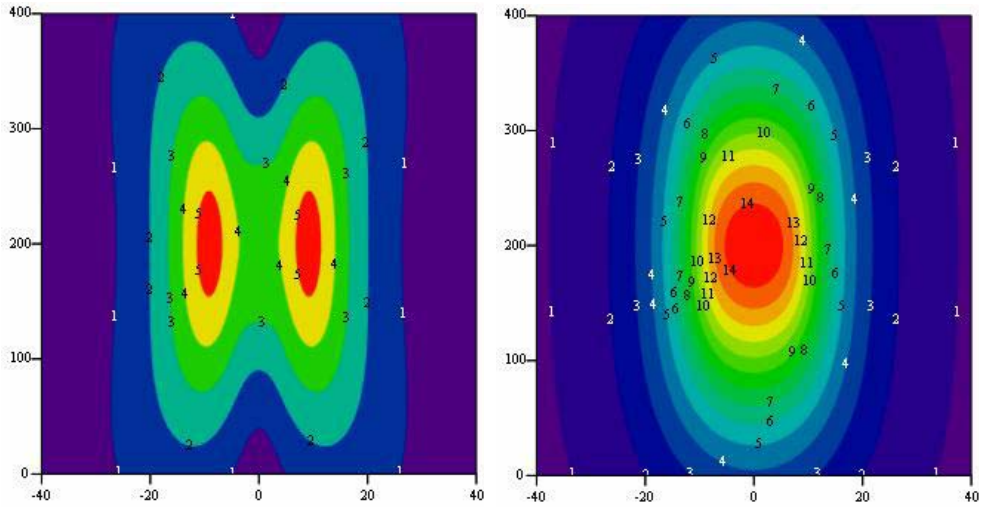

Figure 2. EF (in kV/m, (a) and MF (in μT, (b) distribution in the span of the 330 kV OTL.

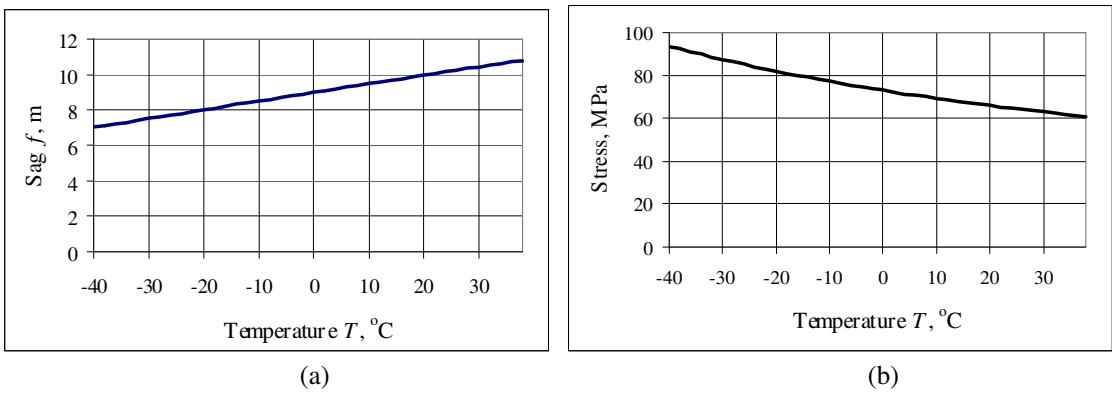

Figure 3. Relationship between sag (a), stress, and temperature for the 330 kV OTL.

4. DISCUSSION

From Table 5, it is evident that among all modes with specific loads that correspond to the possible environmental conditions, the modes with ice and maximum temperature are crucial yield the highest sag.

From Figures 3–7, it is seen that mechanical stresses and wire sags as well as EMF levels vary depending on the temperature. In general, this dependence is linearly proportional. When the temperature increases, the wire extends, the sag and field values expands, while stresses in the wire

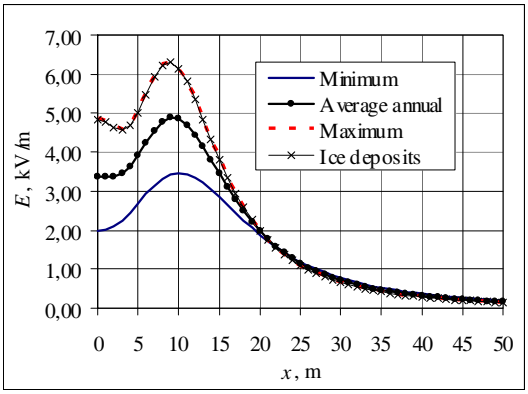

Figure 4. EF distribution in the mid-span of the 330 kV OTL under different environmental conditions.

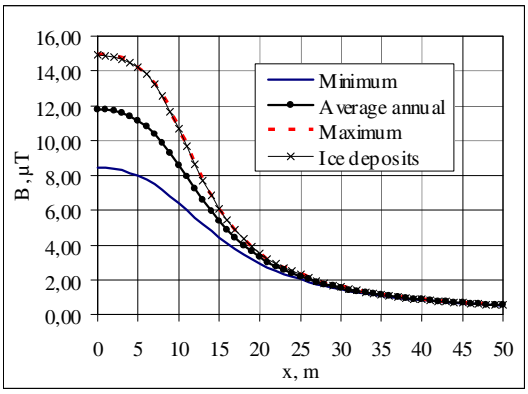

Figure 5. MF distribution in the mid-span of the 330 kV OTL under different environmental conditions.

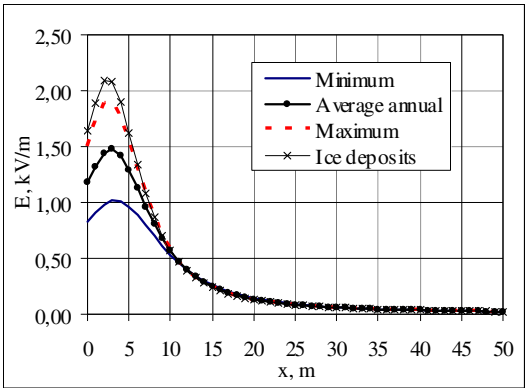

Figure 6. EF distribution in the mid-span of the 110 kV OTL under different environmental conditions.

decreases. With decreasing temperature, we have an opposite situation. The sag and EMF levels at the minimum temperature are the lowest, while stresses in the wire from temperature effects are the highest. Regarding the ice loads, when ice deposits form, vertical and horizontal loads act on the wire. The wire weight with ice deposits grows due to this the sag, and stresses in the wire as well as EMF levels increase.

The highest EMF levels for different classes of OTLs can be under different environmental conditions. For instance, maximum EF intensity and magnetic flux density for the 330 kV line at

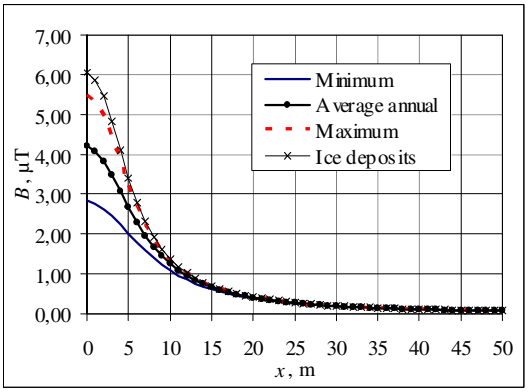

Figure 7. MF distribution in the mid-span of the 110 kV OTL under different environmental conditions.

the maximum temperature and ice deposits are approximately equal. While the highest field levels in the vicinity of the110 kV line are directly found at ice loads.

Therefore, in order to determine the maximum level EMFs, it is necessary to know the highest value of the sag caused the most severe environmental conditions. A comparison of the calculation results for all design modes with specific loads (γ_1–γ_7) and corresponding temperatures can determine the highest sag value. Alternatively, there exists an approach of the critical temperature (for example [12]), which helps to directly find out which conditions give the highest sag. The summary of the approach is confined by comparing the critical temperature t_C, calculated according to Equation (20), with the maximum temperature.

$$t_c = t_{ice} + \frac{\sigma_{ice}}{\alpha E}\left(1 - \frac{\gamma_1}{\gamma_3}\right), \tag{21}$$

where t_{ice} is the temperature during ice formation, °C; σ_{ice} is the stress during ice formation, MPa.

If the maximum temperature is above the critical value, the sag has the highest value at the maximum temperature. If the maximum temperature is lower than the critical value, the maximum sag is found under ice loads.

5. CONCLUSION

EMF levels in the vicinity of two different OTLs were investigated on the basis of an approach considering mechanical loads, wire sag curve, and environmental conditions. It was shown that the highest field levels correspond to the modes with ice and maximum temperature loads. On the assumption that the base level was a value at a temperature of 20°C the difference between the base level and values under different environmental conditions for the 330 kV OTL was varied from −37% (the minimum temperature) to +15% (the maximum temperature) and from −40% (the minimum temperature) to +28% (ice loads) for the 110 kV OTL.

The applied approach and results of the study can be used for the purposes of reducing measurement data to the severe conditions in order to receive the highest EMF value. It can be useful for the direct estimation of electric and magnetic field distributions under OTLs as well.

REFERENCES

1. Moro, F. and R. Turri, "Fast analytical computation of power-line magnetic fields by complex vector method," *IEEE Transactions on Power Delivery*, Vol. 23, No. 2, 1042–1048, 2008.
2. Tzinevrakis, A. E., D. K. Tsanakas, and E. I. Mimos, "Analytical calculation of the electric field produced by single-circuit power lines," *IEEE Transactions on Power Delivery*, Vol. 23, No. 3, 1495–1505, 2008.
3. Ismail, H. M., "Characteristics of the magnetic field under hybrid AC/DC high voltage transmission lines," *Electric Power Systems Research*, Vol. 79, No. 1, 1–7, 2009.

4. Al Salameh, M. S. H. and M. A. S. Hassouna, "Arranging overhead power transmission line conductors using swarm intelligence technique to minimize electromagnetic fields," *Progress In Electromagnetics Research B*, Vol. 26, 213–236, 2010.
5. Mamishev, A. V., R. D. Nevels, and B. D. Russell, "Effects of conductor sag on spatial distribution of power line magnetic field," *IEEE Transactions on Power Delivery*, Vol. 11, 1571–1576, 1996.
6. El Dein, A. Z., "Magnetic-field calculation under EHV transmission lines for more realistic cases," *IEEE Transactions on Power Delivery*, Vol. 24, No. 4, 2214–2222, 2009.
7. Salari, J. C., A. Mpalantinos, and J. I. Silva, "Comparative analysis of 2- and 3-D methods for computing electric and magnetic fields generated by overhead transmission lines," *IEEE Transactions on Power Delivery*, Vol. 24, No. 1, 338–344, 2009.
8. Lucca, G., "Magnetic field produced by power lines with complex geometry," *European Transactions on Electrical Power*, Vol. 21, No. 1, 52–58, 2011.
9. Dezelak K., F. Jakl, and G. Stumberger, "Arrangements of overhead power line phase conductors obtained by differential evolution," *Electric Power Systems Research*, Vol. 81, 2164–2170, 2011.
10. Modric T., S. Vujevic, and D. Lovric, "3D computation of the power lines magnetic field," *Progress In Electromagnetics Research M*, Vol. 41, 1–9, 2015.
11. Keikko, T., "Technical management of the electric and magnetic fields in electric power system," Doctoral Dissertation, Tampere University of Technology, 2003.
12. Kryukov, K. P. and B. P. Novgorodcev, *Construction and Mechanical Calculation of Transmission Lines*, 312, Energiya, Leningrdaskoe otdelenie, Leningrad, 1979 (in Russian).